Journal of Materials Chemistry A

Accepted Manuscript

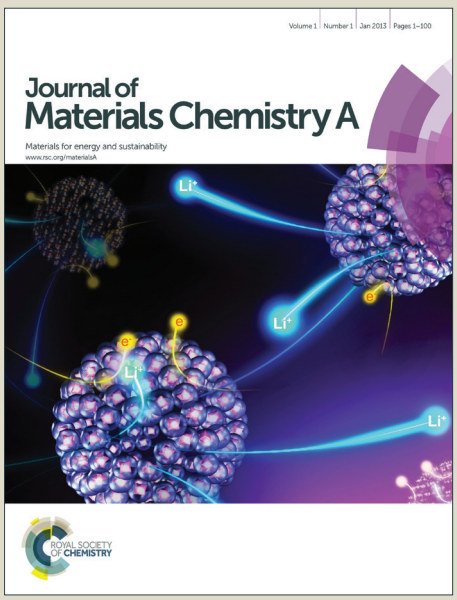

ROYAL SOCIETY OF CHEMISTRY

www.rsc.org/materialsA

Formation of reusable Au-acetonitrile polymers and N-doped graphene catalyst under UV light via submerged liquid plasma process

Jaganathan Senthilnathan, Kodepelly Sanjeeva Rao, Wan-Hsien Lin, Jyh-Ming Ting, Masahiro Yoshimura*

*Promotion Center for Global Materials Research (PCGMR), Department of Material Science and Engineering, National Cheng Kung University, Tainan, Taiwan

Abstract

In this study, acetonitrile polymers (ANPs) synthesized using a submerged liquid plasma (SLP) process were used for the direct reduction of Au^{+3} under ultraviolet (UV) light without the need for reducing or templating agents. Nitrogen-functionalized graphene (NFG) and ANPs, both synthesized via the SLP process were used to form an Au-ANPs-NFG nanohybrid. The pyridinic and pyrrolic nitrogen present in the NFG effectively chemisorbs or binds with ANPs through π-π or σ-π interaction. The ANPs provide excellent control over the Au nanoparticle formation size (~5 nm), as confirmed by high-resolution transmission electron microscopy. High-resolution X-ray photoelectron spectra reveal that the difference in the chemical shift between Au 4f5/2 and Au 4f7/2 peaks was 3.7 eV, which confirms that the reduced form of Au^0 was present in Au-ANPs-NFG. A UV-visible absorbance spectrum further confirms the reduction of Au^{+3} to Au^0 under 254-nm UV light. The catalytic activity of as-synthesized Au-ANPs-NFG was used for the selective oxidation of benzyl alcohol to benzaldehyde in both suspended and immobilized forms. The Au-ANPs-NFG immobilized on Pyrex glass showed 69% conversion of benzyl alcohol to benzaldehyde. The reuse of immobilized Au-ANPs-NFG led to 69%, 64%, and 61% successive conversions with a reaction time of 330 min.

1. Introduction

Graphene and functionalized graphene have been extensively studied for their superior electrical, mechanical, and optical properties.[1-4] Graphene-based nanometal (Pt, Au, Ag, Pd, or Ru) hybrids show great potential for electronics, catalysis, sensors, light-emitting diode, solar cell, medicine, and catalytic applications.[5-13] Au nanoparticles and their hybrids have also been applied as catalytic materials.[14] Previously, a graphene-supported Au hybrid showed a higher chemical stability, lower cost, and higher surface area than those of Au-TiO_2, Au-CeO_2, and Au-SiO_2 metal oxide.[14-15] However, pristine graphene nanometal hybrids lack functional groups and thus the graphene has poor binding and/or holding capacity for the nanometal.[5, 15] In contrast, Au/functionalized graphene hybrids can bind through either non-covalent interactions or chemical bonding, but their long-term stability have not been evaluated.[15] Au nanoparticles encapsulated or stabilized (ex-situ hybridization) with alkyl thiol or 4-dimethylamino pyridine, 2-mercaptopyridine, and bovine serum albumin (amphiphilic biopolymer) have been successfully attached to graphene oxide (GO) or reduced graphene oxide (rGO) surfaces via π-π stacking.[6, 16-19] The main drawback of ex-situ hybridization is low distribution and non-uniformity of the nanoparticles on the graphene or GO domain.[6, 15] In contrast, an in-situ process can provide uniform surface coverage of nanoparticles by controlling the nucleation sites on graphene or GO via surface functionalization.[15] The presence of functional groups (–COOH, –OH, and epoxy) in GO and rGO effectively stabilizes Au nanoparticles. The major drawback of GO or rGO metal hybrids is the presence of oxygen functional groups, which greatly reduces electron mobility due to the presence of sp^3 carbon and limits usage for sensor and other electrical applications.[20] Furthermore, the presence of oxygen functional groups may reduce the catalytic property of Au nanoparticles.[21] Au/functionalized

graphene hybrids (in-situ) have been formed by various methods, such as photochemical reduction,[6] sonolytic reduction,[22] microwave-assisted reduction thermal evaporation,[23] and reduction by hydroxyl-amine,[13] sodium borohydride,[24] amino-terminated ionic liquid,[25] sodium citrate,[26] and ascorbic acid.[27] The synthesis of Au nanoparticles by adding reducing agents is toxic and unsuitable for large-scale production.[28] The reduction and hybridization of Au with functionalized graphene requires a series of steps, including dispersion, filtration, washing, and drying, which considerably increase operation cost.[29] Furthermore, aggregation of Au nanoparticles is typically prevented by the addition of protective agents such as soluble polymers, surfactants, and dendrimers, but this reduces the catalytic performance of the Au nanoparticles.[30] Therefore, eco-friendly and low-temperature synthesis of Au-functionalized graphene hybrids still remains a challenge.[28] Recently, conducting polymers have offered the opportunity for the formation of size-controlled nanometal hybrids.[31] Conductive polymers have been extensively used for applications such as gas storage devices, light harvesting, electrode materials, solar cells, DNA probing, sensors, polymer-based batteries, light-emitting diodes, and supercapacitors.[32-37] Conductive polymers can be formed by the polymerization of a monomer or by modifying a commercially available polymer via the addition and/or replacement of reactive functional groups.[38]

This study synthesized an electron-rich acetonitrile polymers (ANPs), which is used as the bridging material between Au and nitrogen-functionalized graphene (NFG), using the submerged liquid plasma (SLP) process with acetonitrile as the starting material. The ANPs were used as both the reducing and templating agent for the formation of Au nanoparticles, and NFG was used as the base material to facilitate electron transport to

the Au nanoparticles. The catalytic activity of an as-synthesized Au-ANPs-NFG nano hybrid was evaluated by the oxidation of benzylalcohol to benzldehyde under solvent-free conditions. A key impediment for efficient catalytic oxidation is the use of Au nanoparticles in suspended form, which complicates the recovery and reuse of Au nanoparticles due to irreversible agglomeration. Furthermore, Au nanoparticles are quite expensive and their loss increases operation cost. Hence, experiments were performed with both suspended and immobilized forms of the Au-ANPs-NFG catalyst.

2. Materials and methods

2.1 Synthesis of ANPs and NFG in SLP process

In this study, ANPs and NFG were prepared using two different methods. In the first method, etched tungsten (W) needle and a platinum (Pt) sheet were used as the point high-voltage and planar ground electrodes, respectively. The electrode separation distance (~ 100 μm) was controlled by a moving stage assembly (Translation Stage Triple-Divide Series 9064 and 9065) operated by a computer. Acetonitrile (99.95%) procured from Sigma Aldrich was used as the target material. The experiment was conducted in a nitrogen atmosphere to avoid oxygen interference during plasma polymerization. A discharge voltage of 2.7 kV (high-voltage amplifier TREK Model 609E-6) was applied with a repetition rate of 10 kHz, a pulse width of 5 ms, and a pulse delay of 500 μs across the electrodes by using a pulse generator (AVTECH, AV-1022-C). The plasma polymerization was carried out for a fixed reaction time of 420 min and the ANPs were used as both the reducing and stabilizing agent for the formation of Au nanoparticles. The detailed synthesis procedure is given in our previous work.[39] A graphite electrode and a Pt sheet were used for the formation of NFG with a discharge voltage of 2.9 kV. All other conditions were similar to those in

the preceding section. A detailed discussion is given in our previous study.[40]

2.2 Formation of Au-ANPs/NFG hybrid under UV light

The Au-ANPs-NFG hybrid was prepared with various concentrations of ANPs and fixed concentrations of NFG and tetrachloroauric (III) acid ($HAuCl_4$ ions) and exposure to UV light (254 nm) without the addition of any reducing, stabilizing, or capping agents. ANPs (5, 7.5, 10, and 12.5 mg/20 mL) and NFG (5 mg) at the required concentrations were transferred to a quartz beaker and 20 mL of aqueous solution (8 mg/20 mL of Au) of 2 mM $HAuCl_4$ was added. The above solution was kept in the UV chamber with constant stirring at the rate of 50 rpm. The UV-visible absorbance spectrum of the precursor solution was monitored periodically and it was continued until it gets the maximum UV absorbance. A similar reaction was performed with various concentrations of ANPs. Finally, the reduced Au-ANPs-NFG hybrid was centrifuged at 6000 rpm for 15 min and the mixture was washed with acetonitrile to remove excess ANPs. The Au-ANPs-NFG hybrid was suspended in an acetonitrile solvent and used for further characterization. The procedures used for the formation of ANPs, NFG, and Au-ANPs-NFG are given in Fig. 1.

2.3 Characterization

Absorption spectra of Au-ANPs and Au-ANPs-NFG were collected at various time intervals using a UV-visible spectrometer (SCINCO S-3100). A high-resolution transmission electron microscope (HR-TEM, JEOL JEM 2100F) operated at 200 kV was used to examine the microstructure and surface morphology of Au-ANPs-NFG. High-resolution X-ray photoelectron spectroscopy (HRXPS, PHI Quantera SXM, ULVAC Inc., Kanagawa, Japan) was employed to analyze the binding energy of carbon and nitrogen in Au-ANPs-NFG. HRXPS was performed with a monochromatic AlKα

source (25 W, hν = 1486.6 eV) and an energy resolution of 1 eV. All XPS spectra were obtained at a take-off angle of 45° for each element; the atomic sensitivity factors were 0.314, 0.499, and 0.733 for C 1s, N 1s, and O 1s, respectively.

2.4 Immobilization of Au-ANPs-NFG for catalytic application

A Pyrex glass tube with an inner surface area of 4 cm^2 was used for coating the Au-ANPs-NFG catalyst following the procedure mentioned above. To obtain a rough surface, the Pyrex glass tube was treated with 5% (v/v) hydrofluoric acid for 30 min and washed with distilled water and acetone. 4 mL of Au-ANPs-NFG solution (1 mL = 7.5 mg Au-ANPs-NFG) was used for coating the 4-cm Pyrex glass tube. Before coating, the Au-ANPs-NFG suspension was sonicated (under mild conditions) for 5 min and dried in an oven for 30 min at 80 °C. The mass of the coated Au-ANPs-NFG on the Pyrex glass tube was measured at the end of each cycle using a Sartorius microbalance (0-250 mg range) with a sensitivity of 1 µg. Coated Pyrex glass was washed with acetone and reused.

2.5 Catalytic experiments

The catalytic oxidation of benzyl alcohol to benzaldehyde was performed in a round-bottom flask with reflux condenser containing 60 mL of 10 mmol benzyl alcohol (Rankem, India), 40 mmol K_2CO_3 and ~30 mg of Au-ANPs-NFG in water. High pure oxygen from cylinder was constantly purged in to the reaction solution with needle inlet at the rate of 5 mL/min and while stirring at 100 rpm at 60°C for 330 min. The reaction mixture was cooled to room temperature and centrifuged at 2000 rpm. The solution was used for high-performance liquid chromatography (HPLC) analysis (Dionex HPLC model Ultimate 3000). The formation of benzaldehyde was validated with C18 (250 mm × 4.6 mm, 4 µm) analytical columns with a UV detector (at 254 nm) and a mobile

phase that consisted of a mixture of water and acetonitrile (50:50, v/v). An aliquot of 20 μL of diluted samples were injected with a flow rate of 1.0 mL/min.

3. Results and Discussion

3.1 Formation of ANPs and NFG in SLP process

The ANPs were synthesized using acetonitrile as the precursor material in the SLP process.[39] The generation of plasma between the W and Pt electrodes in submerged acetonitrile solvent initiates hydrogen detachment (bond energy values of C-H and -C≡N are 413 and 891 kJ/mol, respectively) in the first step, due to the low bond energy of C-H, leading to the formation of a highly reactive free radical monomer ($^{\cdot}CH_2$-C≡N) (Fig. S1).[39-41] The radicalized monomer ($^{\cdot}CH_2$-C≡N) acts as a building block for the ANPs, where the carbon (predominantly present in sp^2 hybridized form) π bond is localized into nitrogen forming pyrazine. The HPLC/mass spectrometry spectrum of ANPs formed under SLP is given in Fig. 2. The ANPs collected at the end of the reaction showed a major peak with the molecular weight of *m/z* 289 and 4 other peaks of pyrazine (*m/z* 81), pyrazine-2-carbonitrile (*m/z 106*), 1,4,7,9,13-pentaaza-anthracene (*m/z 186*) and 1,4,7,9,13-pentaaza-11-carbonitrile anthracene (*m/z 210*) (Fig. 2). The possible chemical structures of all the compounds were further confirmed with LC/MS/MS analysis and the daughter peaks are identified and given in Table-S1. The mass weight of ANPs depends on the reaction conditions such as plasma intensity, kinetics, and the presence of impurities.[39, 41-43] Different protonated structures of ANPs were formed in different reaction conditions. These structures were not studied further due to the complexity involved in their identification. Hence, the major peak that appeared at *m/z* 289 is considered as that belonging to the ANPs. Possible reaction mechanisms and details of the structure are discussed in our previous study.[39]

A similar experiment was carried out using graphite and platinum electrodes in acetonitrile for the formation of nitrogen-functionalized graphene (NFG). Micro-plasma discharge occurs at the interface and leads to the exfoliation of a punctured radicalized graphene sheet in an acetonitrile solvent.[40] At the same time, free electrons generated during micro-plasma discharge collide with acetonitrile and initiate hydrogen detachment, which results in highly reactive free-radical monomers (·H and $\cdot CH_2\text{-}C\equiv N$).[41, 44] Highly reactive nascent ·H effectively reacts with the punctured radicalized graphene sheet and partially restores the sp^2 network by forming pyridinic (-N=CH-) and pyrrolic (-NH) nitrogen (Fig. S2).[45] The $CH_2\text{-}C\equiv N$ radical present in the solution also initiates the formation of terminal-end aliphatic nitrogen or alkenes ($CH_2\text{-}CH_2\text{-}CN$ or -CH=CH-CH=CH-) in the radicalized graphene layer. Detailed discussions are given in our previous studies.[39-40, 45]

3.2 Effect of ANPs concentration and kinetics on reduction of Au^{+3} ions under UV light

To understand the reduction mechanism, Au^{+3} reduction was carried out on ANPs without adding NFG. ANPs (5.0, 7.5, 10.0, and 12.5 mg/L) and Au^{+3} (fixed) at the required concentrations was placed in a quartz beaker and exposed under UV light for 60 min. The absorbance spectra of Au-ANPs were monitored at 10-min time intervals (Fig. 3a). The wavelength scan measurement shows two distinct peaks, at 360 and 554 nm, respectively. The peak at 360 nm might be due to ANPs or Au-ANPs (Au_{13}) nanoclusters present in the reaction solution, and the peak at 554 nm corresponds to the reduced form of Au nanoparticles.[46] The absorption peak at around 554 nm is attributed to surface plasmon absorption due to the formation of Au nanoparticles. Its absorbance peak increased with increasing ANPs content (from 5.0 to 12.5 mg) (Fig. 4a). Little

change in absorbance was observed beyond 12.5 mg of ANPs, and hence 12.5 mg is considered as the optimum concentration for the formation of Au-ANPs nanoparticles under UV light. To determine the rate of formation, samples were collected every 10 min and the data were fitted with a pseudo-first-order kinetic equation. The plot of $[C/C_0]$ versus t is a straight line with a correlation coefficient (R^2) value of 0.99 and a rate constant (k) of 1.97×10^{-2} min^{-1} (Fig. 4b). The high correlation coefficient indicates that the formation of Au-ANPs under UV light follows pseudo-first-order kinetics. Hence, the rate of reduction depends only on the ANPs concentration (the concentration of Au^{+3} and the UV light intensity were fixed for all the experiments). Similar experimental conditions were used for the formation of Au-ANPs-NFG with a fixed concentration of NFG (5 mg) and various concentrations of ANPs under UV light. The UV-visible spectra of Au-ANPs-NFG show two distinct peaks, at 356 and 548 nm, respectively. With 5 mg of ANPs, there was no significant Au peak, possibly due to the chemisorption of ANPs on the NFG surface (HR-TEM image of NFG is given in Fig. S3). An Au peak appeared at 548 nm when the ANPs concentration was increased to above 5.0 mg and a marginal peak shift was observed when the ANPs concentration was increased from 7.5 to 12.5 mg. Unlike Au^{+3} and ANPs reduction, there was no significant increase in the peak intensities for 7.5, 10, and 12.5 mg of ANPs. This might be due to Au^0 nanoparticles being sandwiched between ANPs and NFG, which hindered their surface plasmon property. The reduction reaction was performed only for 60 min. No significant change was observed when the reaction time was increased to above 60 min. Hence, an irradiation time of 60 min was used for the formation of Au-ANPs-NFG nanohybrid. Furthermore, chemisorbed ANPs on NFG acted as a stabilizing/templating agent for controlling Au nanoparticles. The presence of ANPs on NFG reduced the van der Waals force of attraction (π-π stacking interactions) between

the NFG layers, increasing dispersion in both aqueous and organic solvents. The UV absorption spectra of Au-ANPs and Au-ANPs-NFG are given in Fig. 3a and Fig. 3b, respectively.

3.3 Structural morphology and XPS spectra of Au-ANPs-NFG

The structural morphology of Au-ANPs-NFG hybrid was studied by HR-TEM analysis. Figs. 5a and 5b show HR-TEM images of ANPs and ANPs-NFG hybrid. The image of ANPs is similar to that for polymeric materials, with no shape or orientation. In contrast, ANPs-NFG shows a nested, spherical, or ellipsoidal shape due to the presence of chemisorbed ANPs on NFG (Fig. 5b).[47] The HR-TEM image of the NFG in Fig. 5c shows that the particle size of Au in Au-ANPs-NFG is ~5 nm and that the particles are evenly distributed on the ANPs-NFG surface. The ANPs act as bridges between Au and NFG and effectively control the size of the Au particles; hence, a uniform particle size (~5 nm) was observed throughout the Au-ANPs-NFG surface (Fig. S4). The HR-TEM image of Au-ANPs-NFG shows that the d spacing of Au nanoparticles was 0.24 nm, which corresponds to the (111) plane of a face-centered cubic structure (Figs. 5c, 5d, and 5e). The selected area electron diffraction pattern (SAED) (Fig. 5f) indicates that the Au nanoparticles in Au-ANPs-NFG are nanocrystalline in nature. Furthermore, Fig. 5f shows the ring structure which is a distinctive nature of polycrystalline Au showing 111, 200, 220 and 311 reflections corresponding to face centered cubic Au present in Au-ANPs-NFG.

XPS spectra were recorded to study the surface interaction between Au and ANPs. Figs. 6a and 6b show the XPS spectra of N 1s and Au 4f photoelectrons of Au-ANPs-NFG, respectively. The Au 4f doublet band has binding energies of 82.8 and 86.6 eV, corresponding to Au 4f5/2 and Au 4f7/2 peaks, respectively (Fig. 6a).[48] The difference

in chemical shift between Au 4f5/2 and Au 4f7/2 peaks was 3.7 eV, which confirms the reduced form of Au^0 in Au-ANPs-NFG.[49-50] Similarly, the XPS spectrum of Au-ANPs-NFG shows 8.2% nitrogen. The electronic 1s core levels of N for ANPs-NFG were analyzed and numerically fitted with Gaussian functions. The N 1s region of NFG (Fig. 6b) has three broad peaks, at 398.6, 399.8, and 401.0 eV, respectively, which are attributed to the C-N or -C-NH, -C＝N-, and $-NH_2$ bonds, respectively.[51-53] The nitrogen present in the form of -C＝N- can exist only in the pyridine ring-like structure, which clearly indicates that the addition of Au^{+3} ions and UV light exposure do not alter the basic chemical structure of ANPs and NFG.

3.4 Proposed reaction mechanism for formation of Au with ANPs-NFG under UV light

At the beginning of the reaction, electron-deficient Au^{+3} ions are attracted to electron-rich ANPs. The nucleophilic -C=N-ANPs ligands in ANPs readily donate a lone pair of electrons and form the Au-ANPs (Au^{+3}-N=C-ANPs) coordination complex.[39] When the $[Au^{+3}(\text{-N=C-ANP})_n]Cl_3$ complex is exposed to UV light, active groups in the ANPs can inject photo-excited electrons to the central Au^{+3} ions. The reduced Au^{+2} complex immediately combines with another Au^{+3} ion complex, forming the dimeric complex $[(Au^{+2})_2(\text{-N=C-ANPs})_n]Cl_4$. This dimeric complex undergoes further reduction and forms the stable Au_{13} cluster $[(Au^o\text{-}(Au^+)_{12}(\text{-N=C-ANPs})_n]Cl_{12}$.[46] The central Au in the Au_{13} cluster is in the completely reduced form and surrounded by the Au^+ ANPs complex. The continuous injection of electrons leads to further nucleation and the formation of stable ~5-nm particles. The proposed reduction mechanism of Au^{+3} ions under UV light by ANPs-NFG is given in Fig. 7.

3.5 Catalytic activity of immobilized Au-ANPs-NFG

The use of an eco-friendly oxidizing agent, such as H_2O_2 or O_2 in aqueous solution, is one of the most attractive and economically viable solutions for the formation of benzaldehyde from benzyl alcohol.[54] The oxidation of benzyl alcohol to benzaldehyde has been extensively carried out with Au nanoparticles as catalyst.[54-56] The major shortcoming of this process is (a) Au nanoparticles are very expensive, (b) complete recovery of the catalyst at the end of the reaction is difficult, (c) stirring or mechanical agitation can destabilize the Au nanoparticles, making them detach from the binding material, (d) the agglomeration of Au or support materials such as graphene oxide, reduced graphene oxide, and polymeric materials may occur at the end of the reaction, and (e) nanoparticles are difficult to remove from the end solution even after centrifugation or filtration. To overcome these difficulties, the oxidation of benzyl alcohol to benzaldehyde was carried out with both suspension and immobilized forms of Au-ANPs-NFG. Furthermore, the catalytic reaction of Au-ANPs-NFG was evaluated in the absence of an organic solvent. The reaction kinetics and HPLC chromatogram of the oxidation of benzyl alcohol to benzaldehyde with immobilized Au-ANPs-NFG is given in Figs. 8 and 9. Identical conditions were maintained for both suspended and immobilized forms of Au-ANPs-NFG catalyst. The catalyst used in suspended form had a conversion rate of 89% after 60 min of reaction time. Immobilized Au-ANPs-NFG had a conversion rate of only 69% at the end of the reaction time (Fig. 8). Only marginal conversion was observed beyond the fixed reaction time of 330 min. The decrease in the conversion rate for the immobilized Au-ANPs-NFG might be due to the reduction of the surface area and/or contact time of the Au nanoparticles.[57] In comparison, the suspended Au-ANPs-NFG has more surface area and contact time and thus a higher conversion rate.

The ANPs-NFG injects electrons into the Au surface and subsequently electrons are transferred to dissolved oxygen present in the solution and form $^{-}O=O$ ions (Fig. 9). The ionized oxygen molecules oxidize benzyl alcohol, forming benzaldehyde.[57] The controlled injection of oxygen ions to the benzyl alcohol controls the further oxidation of benzaldehyde.[57] The immobilized Au-ANPs-NFG was reused for up to three cycles with identical conditions.[58] Only marginal reduction in efficiency was observed (69%, 64%, and 61% for the 1st, 2nd, and 3rd cycles, respectively) (Fig. 8). The comparisons of catalytic activity of Au-ANPs-NFG with previous reported works are listed in Table-1. The immobilized Au-ANPs-NFG hybrid shows promising catalytic activity towards the solvent-free oxidation of benzyl alcohol presence of oxygen with excellent selectivity and yields.

4. Conclusion

A sustainable and eco-friendly SLP process was used for the formation of Au-ANPs-NFG hybrid under UV light. The reduction of Au nanoparticles in the presence of ANPs under UV light was confirmed by UV-visible spectra and XPS analysis. The ANPs effectively limits the size of Au nanoparticles to ~5 nm, whilst the Au particles were uniformly distributed on the ANPs-NFG surface. The 5 nm Au nanoparticles confined within ANPs-NFG were shown to exhibit excellent catalytic performance for the oxidation of benzyl alcohol to benzaldehyde by O_2 in the aqueous state. They were also found to be reusable, whereby the conversion rate of immobilized Au-ANPs-NFG remained almost unchanged for three successive cycles. All previous studies reported that the high temperatures were required for calcinating the Au catalyst hybrid, whereas in this study we demonstrate the fabrication of Au-ANPs-NFG catalyst

under UV light at only ambient temperatures. Furthermore immobilized Au-ANPs-NFG could be used for organic synthesis, high-performance supercapacitor, energy storage, sensor, and solar cell applications.

Acknowledgements

The authors are grateful to Prof. Jiunn-Der Liao (Department of Material Science and Engineering, NCKU) and Dr. Chih-Chiang Weng for experimental help and discussions. HR-TEM, SEM, EDX, and Raman spectroscopy analysis were performed at the Department of Material Science, National Cheng Kung University Tainan, Taiwan.

References

[1]. K. S. Novoselov, A. K. Geim, S. V. Morozov, D. Jiang, Y. Zhang, S. V. Dubonos, I. V. Grigorieva and A. A. Firsov, *Science,* 2004, **306,** 666-669

[2]. K. S. Novoselov, V. I. Fal'ko, L. Colombo, P. R. Gellert, M. G. Schwab, K. Kim, *Nature,* 2012, **490,** 192-200.

[3]. R. Ruoff, *Nat. Nanotech.,* 2008, **3,** 10-11.

[4]. F. Bonaccorso, A. Lombardo, T. Hasan, Z. Sun, L. Colombo and A. C. Ferrari, *Mater. Today,* 2012, **15,** 564-589.

[5]. S.S.J. Aravind, V. Eswaraiah and S. Ramaprabhu, *J. Mater. Chem.,* 2011, **21,** 17094-17097.

[6]. X. Huang, X. Qi, Y. Huang, S. Li, C. Xue, C. L. Gan, F. Boey and H. Zhang, *ACS Nano,* 2010, **4,** 6196–6202.

[7]. M. Haruta, *Nature,* 2005, **437,** 1098–1099.

[8]. R. Murray, *Chem. Rev.* 2008, **108,** 2688–2720.

[9]. K. Sanjeeva Rao, J. Sentilnathan, H-W. Cho, J-J Wu and M. Yoshimura, *Adv. Funct. Mater.,* 2014, doi:10.1002/adfm.201402621

[10]. M.D. Hughes, Y-J. Xu, P. Jenkins, P. McMorn, P. Landon, D.I. Enache, A.F. Carley, G.A. Attard, G.J. Hutchings, F. King, E.H. Stitt, P. Johnston, K. Griffin and C.J. Kiely, *Nature,* 2005, **437,** 1132–1135.

[11]. M.R. Jones, K. D. Osberg, R. J. Macfarlane, M. R. Langille and C. A. Mirkin, *Chem. Rev.,* 2011, **111,** 3736–3827.

[12]. C. M. Cobley, J. Chen, E. C. Cho, L. V. Wang and Y. Xia, *Chem. Soc. Rev.,* 2010, **40,** 44–56.

[13]. C-Y. Chen, C-Y. Fan, M-T. Lee and J-K. Chang, *J. Mater. Chem.,* 2012, **22,** 7697-7700.

[14]. X. Xie, J. Long, L. Chen, Y. Wang, Z. Zhang and X. Wang, *RSC Adv.,* 2012, **2,** 12438- 12446.

[15]. X. Huang, X. Qi, F. Boey and H. Zhang, *Chem. Soc. Rev.,* 2012, **41,** 666-686.

[16]. J. Liu, S. Fu, B. Yuan, Y. Li and Z. Deng, *J. Am. Chem. Soc.,* 2010, **132,** 7279-7281.

[17]. D. Wei and W. Qian, *Colloids Surf. B,* 2008, **62,** 136-142.

[18]. N.R. Jana, L. Gearheart and C. J. Murphy, *Chem. Mater.,* 2001, **13,** 2313-2322.

[19]. X. Wang, G. Meng, C. Zhu, Z. Huang, Y. Qian, K. Sun, and X. Zhu, *Adv. Funct. Mater.,* 2013, **23,** 5771-5777.

[20]. M. Inagaki, Y.A. Kim and M. Endo, *J. Mater. Chem.,* 2011, **21,** 3280-3292.

[21]. D. A. Bulushev, I. Yuranov, E.I. Suvorova, P. A. Buffat, and L. Kiwi-Minsker, *J. Catal.,* 2004, **224,** 8-17.

[22]. K. Vinodgopal, B. Neppolian, I. V. Lightcap, F. Grieser, M. Ashokkumar, and P. V. Kamat, *J. Phys. Chem. Lett.,* 2010, **1,** 1987–1993.
[23]. H. Q. Zhou, C. Y. Qiu, Z. Liu, H. C. Yang, L. J. Hu, J. Liu, H. F. Yang, C. Z. Gu and L. F. Sun, *J. Am. Chem. Soc.,* 2010, **132,** 944-946.
[24]. R. Muszynski, B. Seger, and P. V. Kamat, *J. Phys. Chem. C,* 2008, **112,** 5263-5266.
[25]. F. Li, H. Yang, C. Shan, Q. Zhang, D. Han, A. Ivaskab and L. Niu, *J. Mater. Chem.,* 2009, **19,** 4022-4025.
[26]. K. Sanjeeva Rao, J. Senthilnathan, J-M. Ting and M. Yoshimura, *Nanoscale*, 2014, **6,** 12758-12768.
[27]. Y.-K. Kim, H.-K. Na, Y. W. Lee, H. Jang, S. W. Han and D.-H. Min, *Chem. Commun.,* 2010, **46,** 3185-3187.
[28]. M.J. Kim, Y. Jeong, S. Sohn, S. Y. Lee, Y. J. Kim, K. Lee, Y. H. Kahng and J-H. Jang, *AIP Adv.,* 2013, **3,** 012117.
[29]. Z. Liu, X. Duan, G. Qian, X. Zhou and W. Yuan, *Nanotech.,* 2013, **24,** 045609.
[30]. S. Dong, C. Tang, H. Zhou and H. Zhao, *Gold Bull.,* 2004, **37,** 3-4.
[31]. M. Ates, *Mater. Sci. Eng. C,* 2013, **33,** 1853-1859.
[32]. S. Wang, B.S. Gaylord and G.C. Bazan, *J. Am. Chem. Soc.,* 2004, **6,** 5446-5451.
[33]. H.D. Tran, D. Li and R.B. Kaner, *Adv. Mater.,* 2009, **21,** 1487-1499.
[34]. A. Patra and U. Scherf, *Chem. Eur. J.,* 2012, **18,** 10074-10080.
[35]. L. Nyholm, G. Nyström, A. Mihranyan and M. Strømme, *Adv. Mater.,* 2011, **23,** 3751-3769.
[36]. T. Janoschka, M.D. Hager and U.S. Schubert, *Adv. Mater.,* 2012, **24,** 6397-6409.
[37]. C.C. Cheng, Y.L. Chu, P.H. Huang, Y.C. Yen, C.W. Chu, A.C.M. Yang, F.H. Ko, J.K. Chen and F.C. Chang, *J. Mater. Chem.,* 2012, **22,** 18127-18131.
[38]. J. Chen, P. Zhang, G. Fang, P. Yi, X. Yu, X. Li, F. Zeng and S. Wu, *J. Phys. Chem. B,* 2011, **115,** 3354-3362.
[39]. J. Senthilnathan, C.C. Weng, J.-D. Liao and M. Yoshimura, *Sci. Rep.,* 2013, **3,** 2414-2420.
[40]. J. Senthilnathan, K. S. Rao and M. Yoshimura, *J. Mater. Chem. A,* 2014, **2,** 3332-3337.
[41]. N. Inagaki, S. Tasaka and Y. Yamada, *J. Polym. Sci. Part A Polym. Chem.,* 1992, **30,** 2003-2010.
[42]. H. Wang and M. Yoshimura, *Chem. Phys. Lett.,* 2001, **348,** 7-10.
[43]. T. Watanabe, H. Wang, Y. Yamakawa and M. Yoshimura, *Carbon,* 2006, **44,** 799-823.
[44]. N. Inagaki, Plasma surface modification and plasma polymerization, Technomic Publishing Company, Lancaster, PA, **1996.**

[45]. J. Senthilnathan, Y-.F. Liu, K.S. Rao and M. Yoshimura, *Sci. Rep.,* 2014, **4,** 4395-4401.

[46]. Y. Shichibu, K. Suzuki and K. Konishi, *Nanoscale,* 2012, **4,** 4125-4129.

[47]. J. Ortiz-Medina, M.L. García-Betancourt, X. Jia, R. Martínez-Gordillo, M.A. Pelagio-Flores, D. Swanson, A.L. Elías, H.R. Gutiérrez, E. Gracia-Espino, V. Meunier, J. Owens, B.G. Sumpter, E. Cruz-Silva, F.J. Rodríguez-Macías, F. López-Urías, E. Muñoz-Sandoval, M.S. Dresselhaus, H. Terrones and M. Terrones, *Adv. Funct. Mater.,* **2013**, *23,* 3755-3762.

[48]. S-S. Kim, Y-R. Kim, T.D. Chung and B-H. Sohn, *Adv. Funct. Mater.,* 2014, **24,** 2764-2771.

[49]. M. Behera and S. Ram, *Appl. Nanosci.,* 2014, **4,** 247–254.

[50]. M.K. Abyaneh, D. Parmanik, S. Varma, S.W. Gosavi and S.K. Kulkarni, *J. Phys. D Appl. Phys.,* 2007, **40,** 3771–3779.

[51]. J. Senthilnathan, K.S. Rao, W-H Lin, J.-D. Liao and M. Yoshimura, *Carbon,* 2014, **78,** 446-454.

[52]. P. Dementjev, A. de-Graaf, M.C.M. van-de Sanden, K.I. Maslakov, A.V. Naumkin and A. A. Serov, *Diam. Relat. Mater.,* 2000, **9,** 1904-1907.

[53]. A. Johansson and S. Stafstrom, *J. Chem. Phys.,* 1999, **111,** 3203-3208.

[54]. V.R. Choudhary, R. Jha and P. Jana, *Green Chem.,* 2007, **9,** 267–272.

[55]. V.R. Choudhary, D.K. Dumbre, B.S. Uphade and V.S. Narkhede, *J. Mol. Catal. A Chem.,* 2004, **215,** 129-135.

[56]. P. Sharma, G. Darabdhara, T. Muralikrishna Reddy, A. Borah, P. Bezboruah, P. Gogoi, N. Hussain, P. Sengupta and M.R. Das, *Catal. Comm.,* 2013, **40,** 139–144.

[57]. T.A.G. Silva, E.T.-N. Núria López and L.M. Rossi, *Sci. Reps.,* 2014, **4,** 05766.

[58]. Y. Liu, H. Tsunoyama, T. Akita and T. Tsukuda, *J. Phys. Chem. C,* 2009, **113,** 13457.

[59]. C.Y. Ma, B.J. Dou, J.J. Li, J. Cheng, Q. Hu, Z.P. Hao and S.Z. Qiao, *Appl. Catal. B: Env.,* 2009, **92,** 202-208.

[60]. H. Sun, Q. Tang, Y. Du, X. Liu, Y. Chen and Y. Yang, *J. Colloid Interf. Sci.,* 2009, **333,** 317-323.

[61]. Y. Chen, H. Lim, Q. Tang, Y. Gao, T. Sun, Q. Yan and Y. Yang, *Appl. Catal. A: Gen.,* 2010, **380,** 55-65.

[62]. J. Hu, L. Chen, K. Zhu, A. Suchopar and R. Richards, *Catal. Today,* 2007, **122,** 277-283.

[63]. A. Villa, N. Janjic, P. Spontoni, D. Wang, D. S. Su and L. Prati, *Appl. Catal. A: Gen.,* 2009, **364,** 221-228.

[64]. N.Q. Long and N.A. Quan, *Reac. Kinet. Mech. Cat.,* 2014, doi:10.1007/s11144-014-0773-4.

[65]. V. R. Choudhary, R. Jha, and P. Jana, *Green Chem.,* 2007, **9,** 267-272.

[66]. P. Sharma, G. Darabdhara, T.M. Reddy, A. Borah, P. Bezboruah, P. Gogoi, N. Hussain, P. Sengupta and M.R. Das, *Catal. Comm*., 2013, **40,** 139-144.

[67]. X. Xie, J. Long, J. Xu, L. Chen, Y. Wang, Z. Zhang and X. Wang, *RSC Adv.,* 2012, **2,** 12438-12446.

Figure Captions

Fig. 1 Proposed mechanism for formation of Au-ANPs-NFG under UV light (a) Formation of ANPs under SLP condition, (b) formation of NFG under SLP condition, and (c) formation of Au-ANPs-NFG under UV light

Fig. 2 LC/MS spectra of ANPs samples collected at the end of the reaction. (a) Pyrazine, (b) pyrazine-2-carbonitrile, (c) 1,4,7,9,13-pentaaza-anthracene, and (g) 1,4,7,9,13-pentaaza-11-carbonitrile anthracene.

Fig. 3 (i) UV-visible absorption properties for fixed concentration of Au^{3+} and different concentrations of ANPs. (ii) UV-visible absorption properties for fixed concentrations of Au^{3+} and NFG and various concentrations of ANPs.

Fig. 4 (a) Comparison of Au reduction with various concentrations of ANPs exposed under UV light. (b) Reaction rate and order of Au reduction under UV light with optimum concentration of Au:ANPs; inset shows various concentration of ANPs exposed under UV light (1) water used as blank (2) 5.0 mg (3) 7.5 mg (4) 10 mg (5) 12.5 mg and (6) 15.0 mg

Fig. 5 HR-TEM images of (a) ANPs, (b) ANPs-NFG, and (c-e) Au-ANPs-NFG nanoparticles. (f) SAED pattern of Au-ANPs-NFG nanoparticles.

Fig. 6 (a) XPS N 1s spectrum of Au-ANPs-NFG. (b) Au 4f core level XPS spectrum of Au-ANPs-NFG hybrid.

Fig. 7 Proposed reaction mechanism of formation of Au nanoparticles under UV light assisted by ANPs-NFG

Fig. 8 Conversion of benzyl alcohol to benzaldehyde by suspended and immobilized Au-ANPs-NFG. Note: Sus.- suspended form of Au-ANPs-NFG catalyst; Imm.- immobilized form of Au-ANPs-NFG catalyst

Fig. 9 HPLC spectra of conversion of benzyl alcohol to benzaldehyde with immobilized Au-ANPs-NFG catalyst. (a) Initial concentration of benzaldehyde, (b) concentration of benzaldehyde after reaction time of 40 min, and (c) concentration of benzaldehyde at end of reaction

Table 1: Selective oxidation of benzyl alcohol to benzaldehyde in the presence of Au nanohybrid

S.No	Catalysts	Stabilizer	Temp.	Au size	Conversion	Ref.
Present study		ANPs	60 °C	5 nm	69% (immobilized form)	
Present study		ANPs	60 °C	5 nm	89% (suspended form)	
1	Au-Pd	SBA-15	200°C	10-50 nm	20.5%	[59]
2	Au	SBA 16	110 °C	5-6 nm	19.3%	[60]
3	Au5Pd/S16	SBA 16	400 °C	6-6.2 nm	22.3%	[61]
4	Au	GMS	500°C	6.2 nm	95%	[62]
5	Au-SBA 20	TPP	200°C	<1 nm	94%	[58]
6	Au-Pd	-	100 °C	12-15 nm	87.7%	[57]
7	Au-Pd	PVA	-	~3.9 nm	90%	[63]
8	Au/γ-Al_2O_3	S823	550 °C	9.4 nm	44.5%	[64]
9	Au/U_3O_8	-	400 °C	12.2 nm	53%	[65]
10	Au	GO	MW	2-20 nm	77%	[66]
11	Au	Graphene	120 °C	2-20 nm	67%	[67]

*ANPs: Acetonitrile polymers; SBA 16: Mesoporous Silica; GMS: Gold mesoporous silica; TPP: Triphenylphosphine; PVA: Polyvinyl alcohol; GO: Graphene oxide

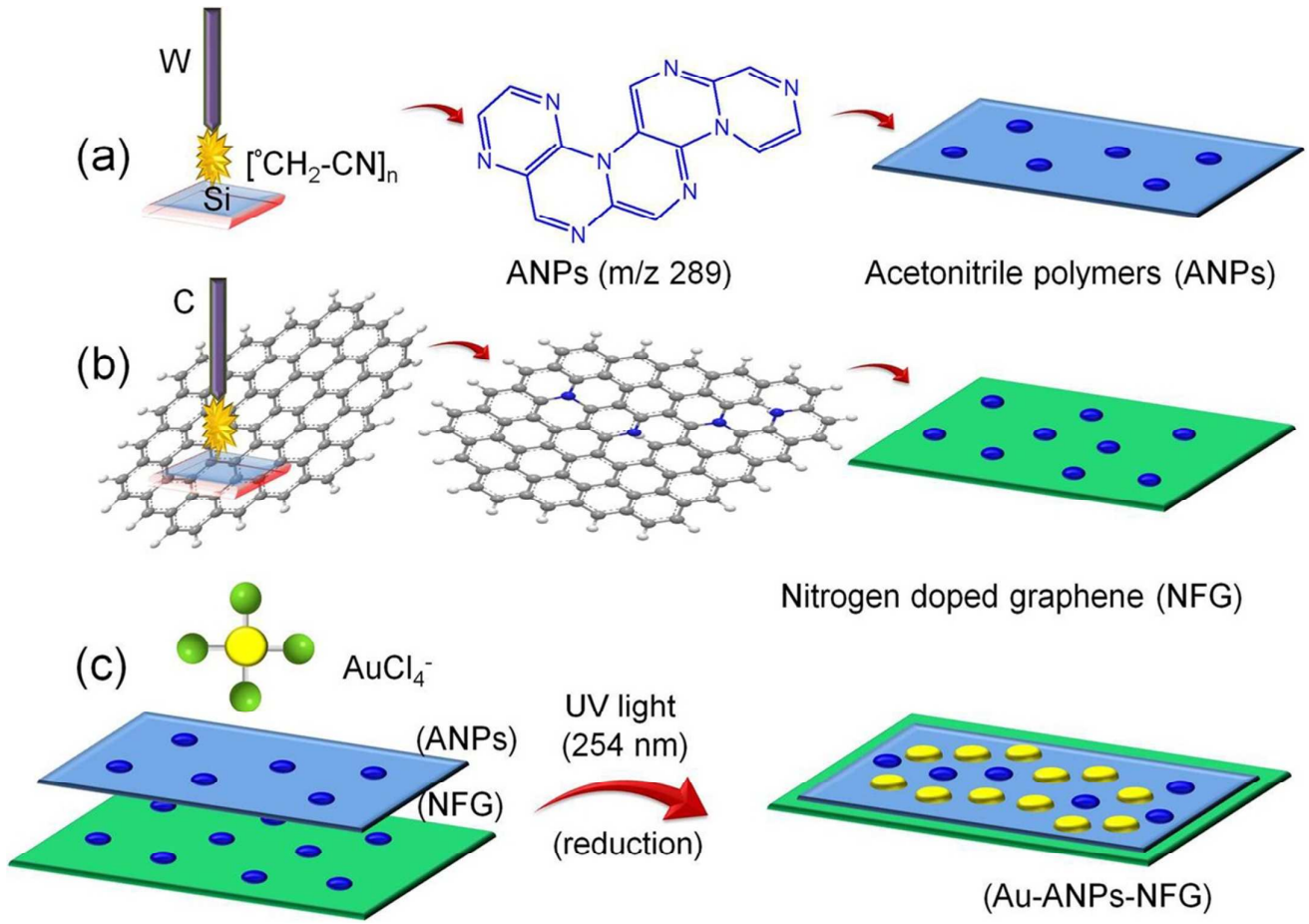

Fig. 1

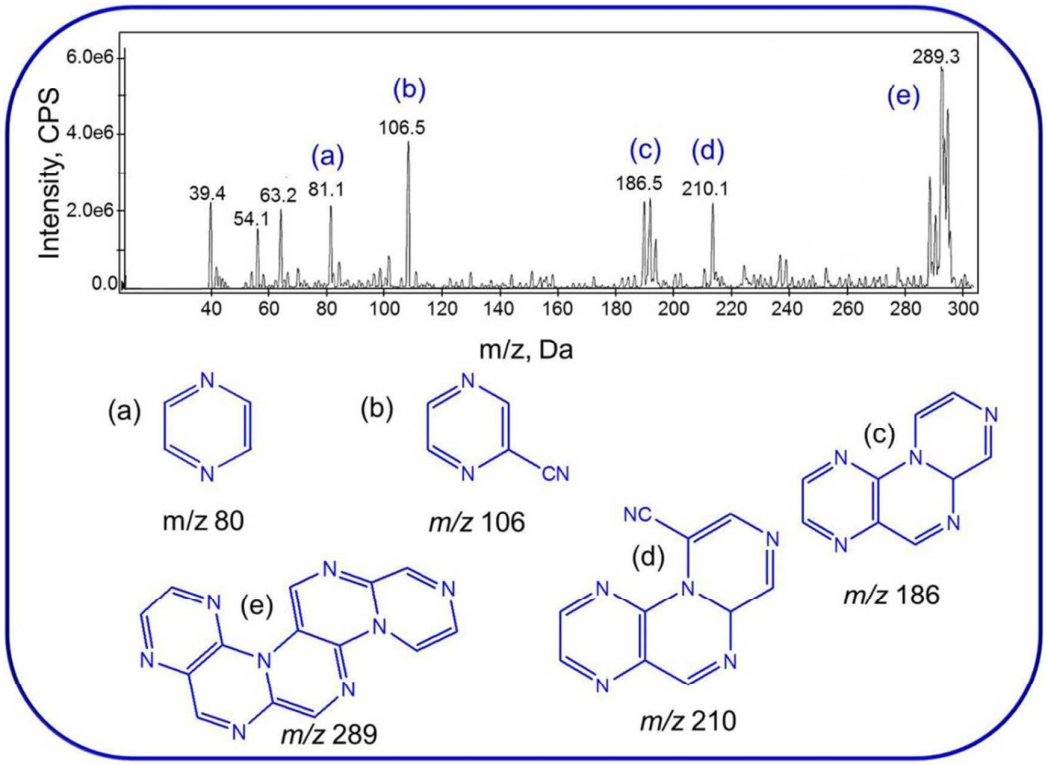

Fig. 2

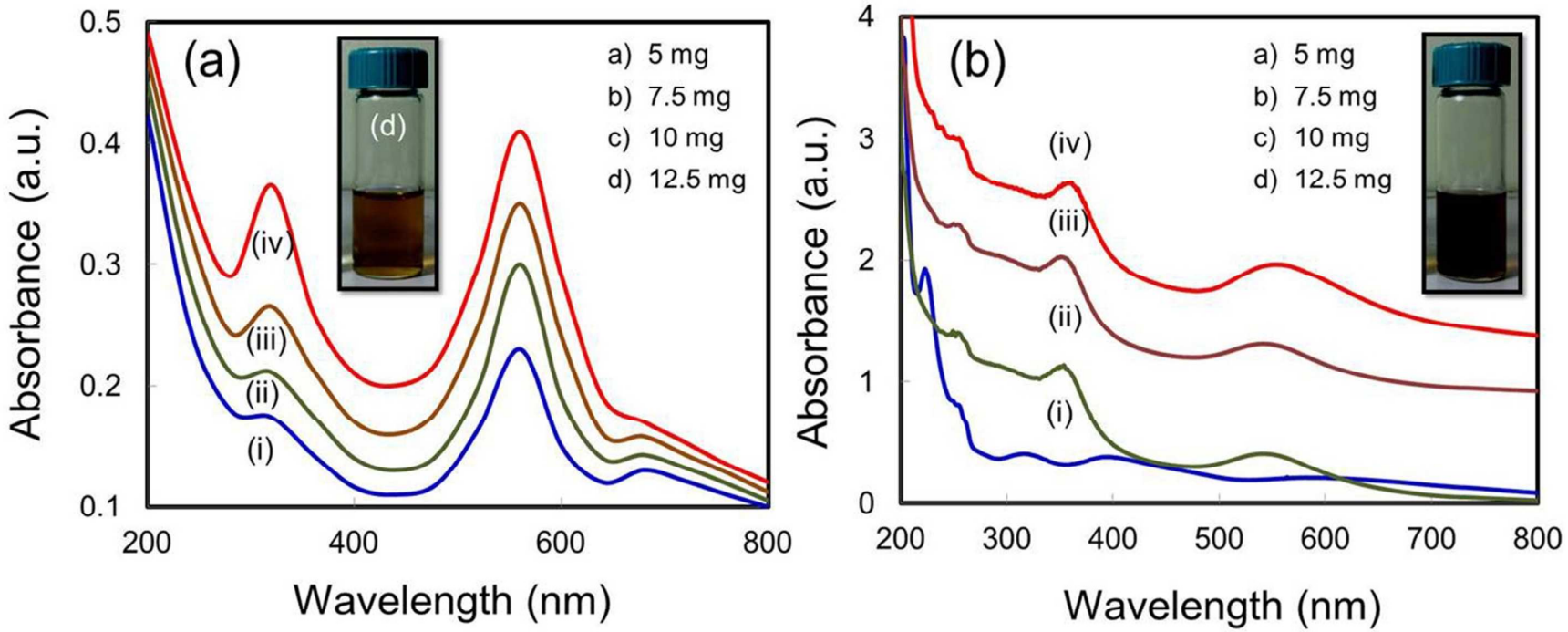

Fig. 3

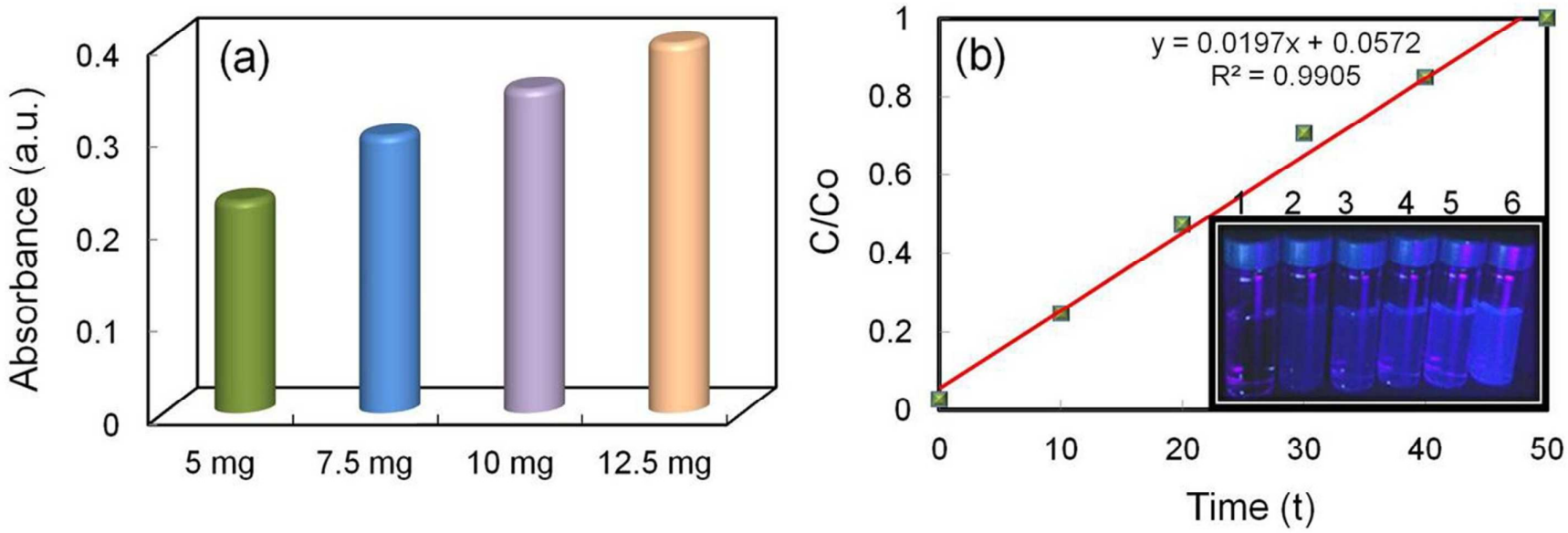

Fig. 4

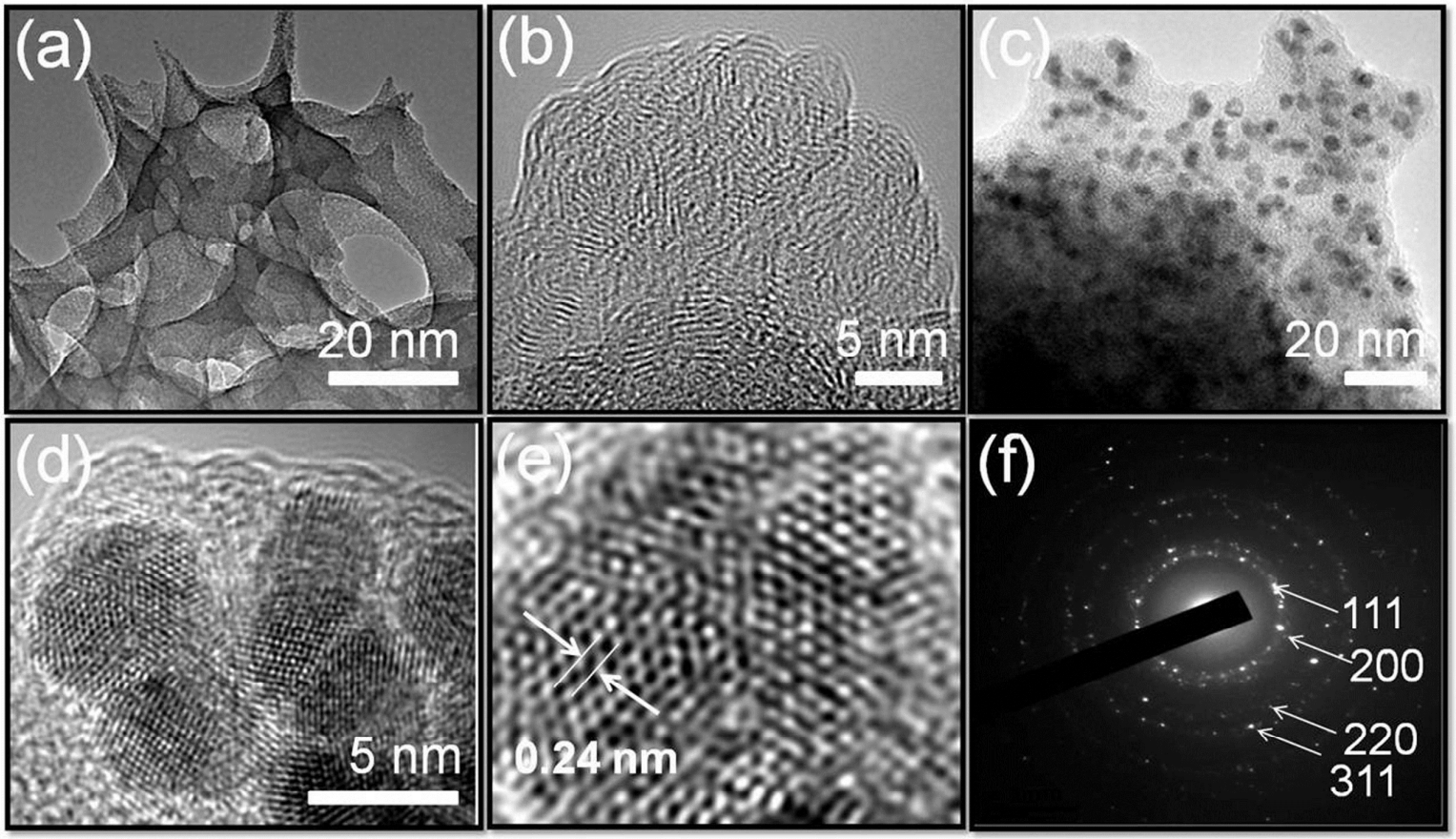

Fig. 5

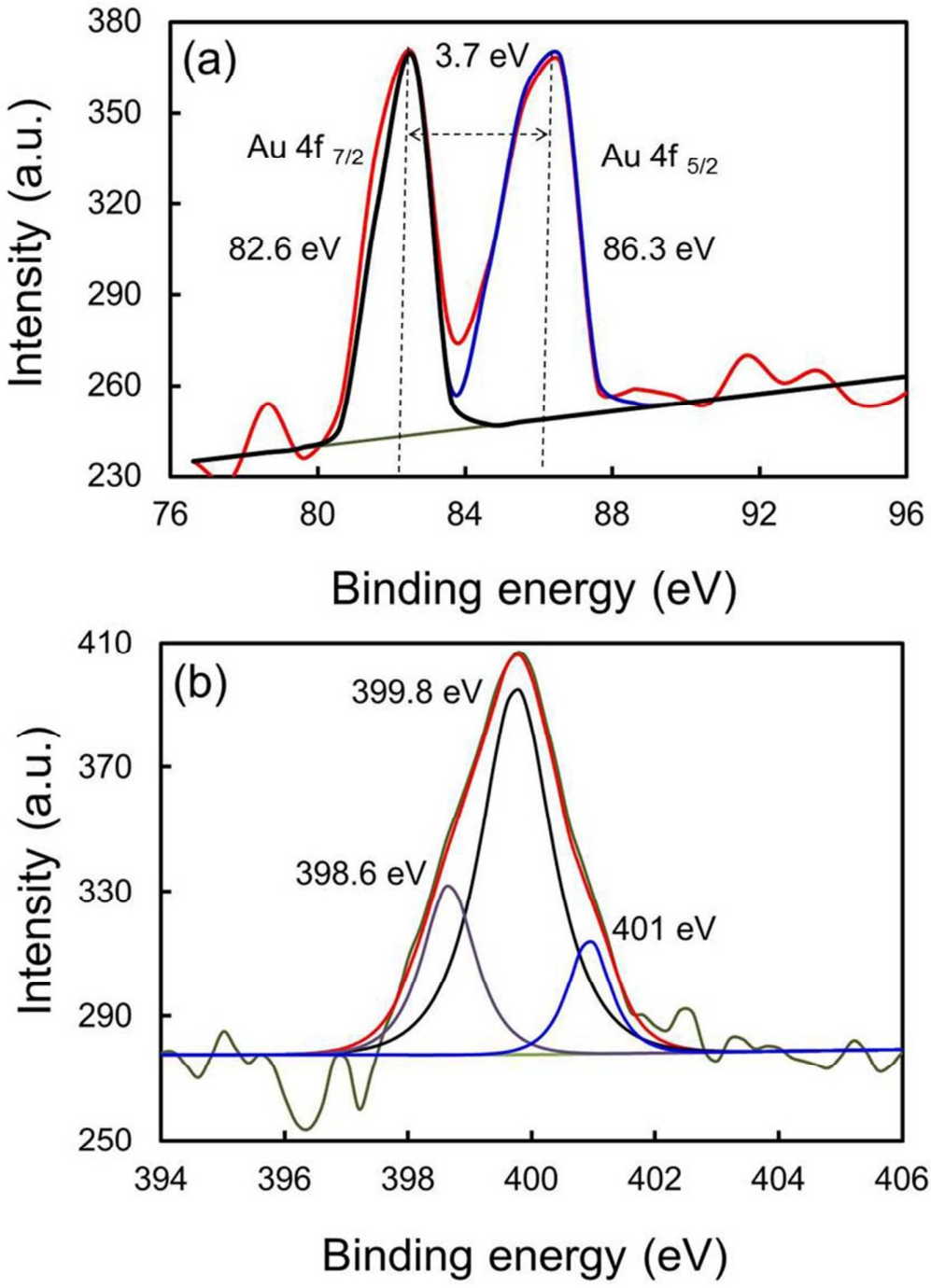

Fig. 6

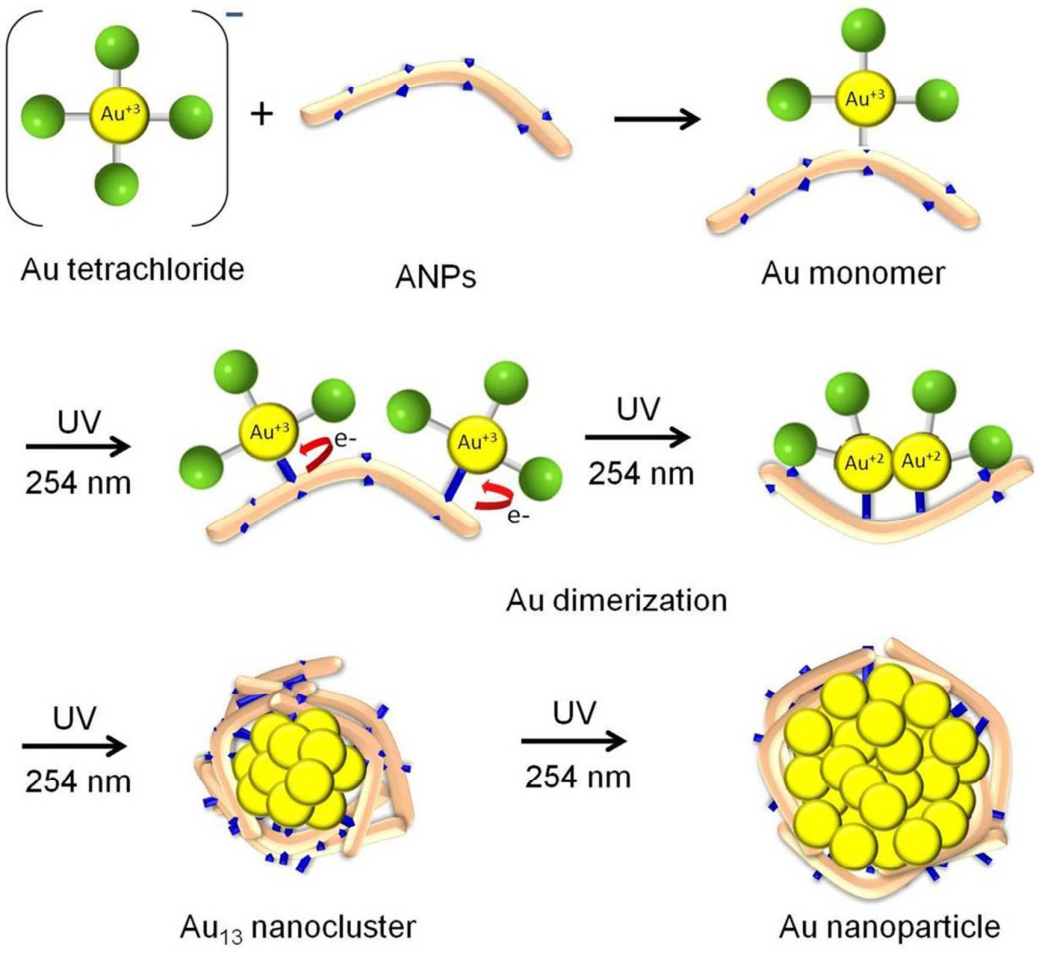

Fig. 7

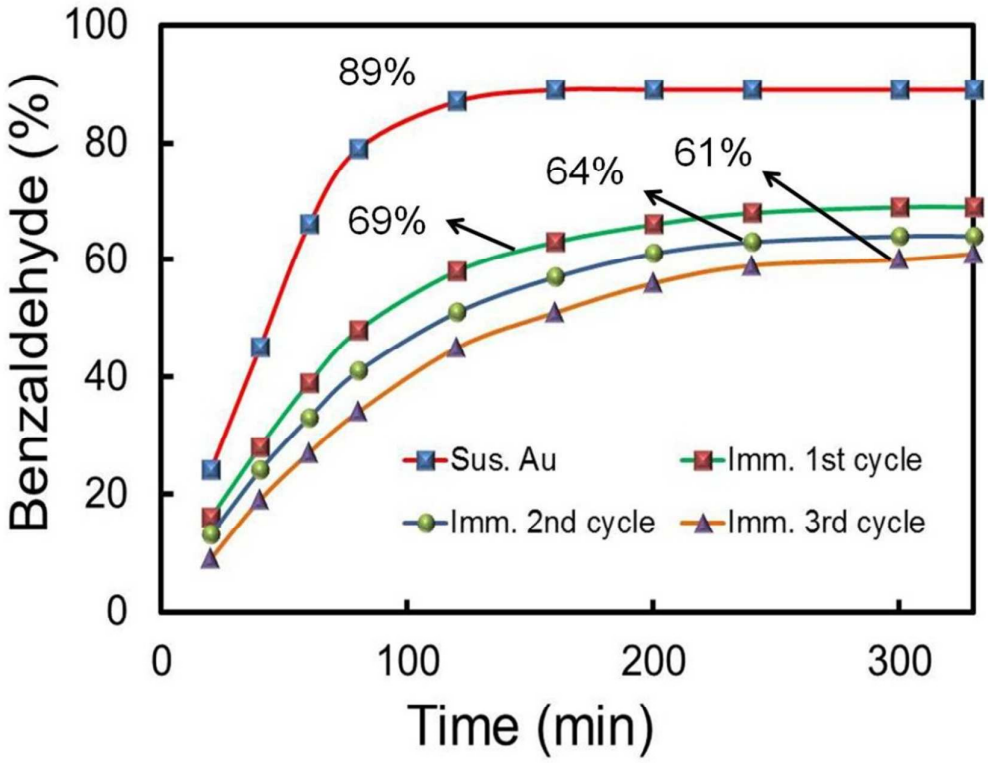

Fig. 8

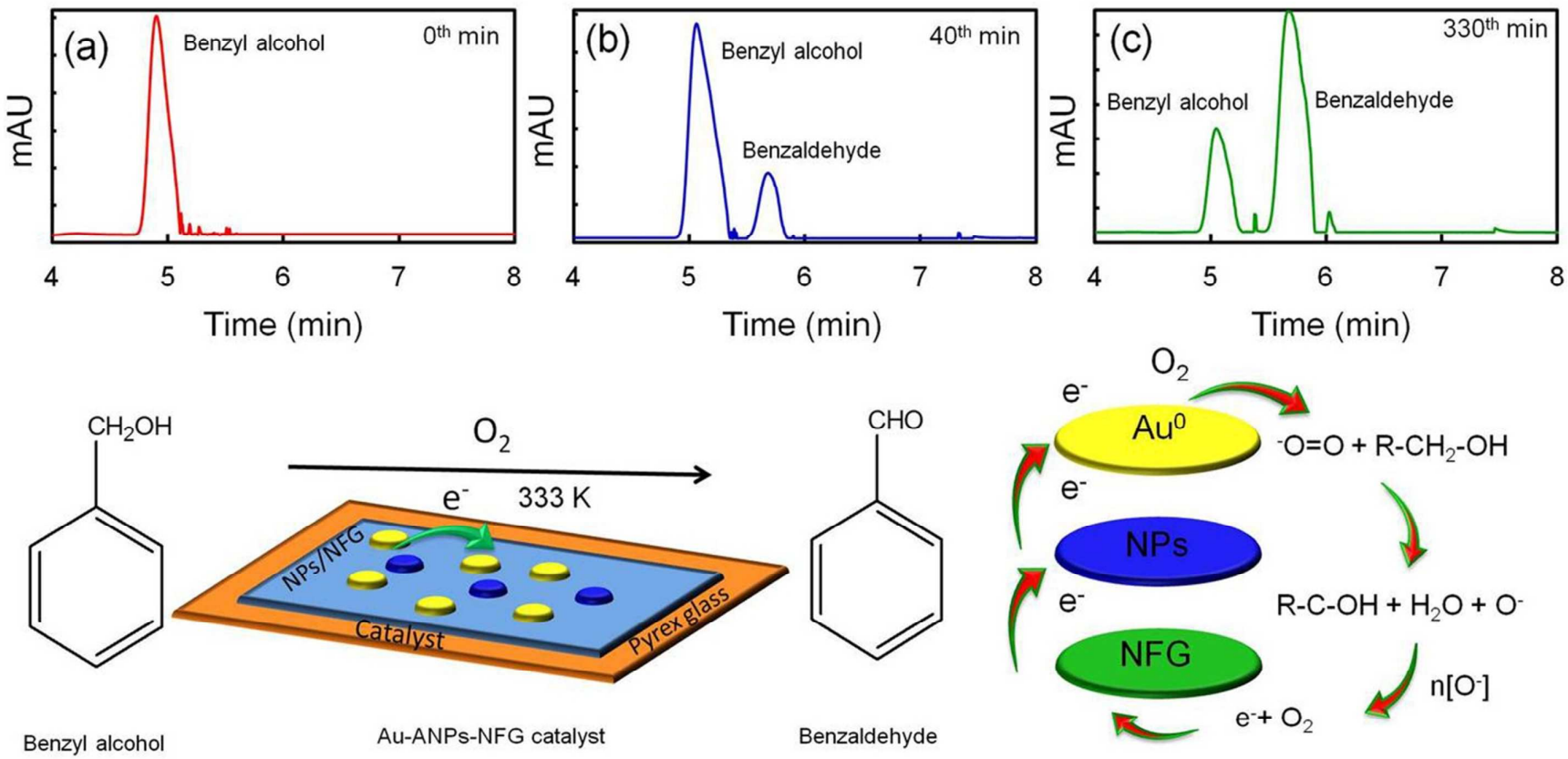

Fig. 9